

Myocardial motion and deformation patterns in an experimental swine model of acute LBBB/CRT and chronic infarct

Nicolas Duchateau · Marta Sitges · Adelina Doltra · Juan Fernández-Armenta · Nuria Solanes · Montserrat Rigol · Luigi Gabrielli · Etelvino Silva · Aina Barceló · Antonio Berruezo · Lluís Mont · Josep Brugada · Bart Bijnens

Received: 8 November 2013 / Accepted: 15 March 2014 / Published online: 21 March 2014
© Springer Science+Business Media Dordrecht 2014

Abstract In cardiac resynchronization therapy (CRT), specific changes in motion/deformation happen with left-bundle-branch-block (LBBB) and following treatment. However, they remain sub-optimally studied. We propose a two-fold improvement of their characterization. This includes controlling them through an experimental model and using more suitable quantification techniques. We used a swine model of acute LBBB and CRT with/without chronic infarct (pure-LBBB: N = 11; LBBB + left-anterior-descending infarct: N = 11). Myocardial displacement, velocity and strain were extracted from short-axis echocardiographic sequences using 2D speckle-tracking. The data was transformed to a single spatiotemporal system of coordinates to perform subject comparisons and quantify pattern changes at similar locations and instants. Pure-LBBB animals showed a specific intra-ventricular dyssynchrony pattern with LBBB (11/11 animals), and the

recovery towards a normal pattern with CRT (10/11 animals). Pattern variability was low within the pure-LBBB population, as quantified by our method. This was not correctly assessed by more conventional measurements. Infarct presence affected the pattern distribution and CRT efficiency (improvements in 6/11 animals). Pattern changes correlated with global cardiac function (global circumferential strain) changes in all the animals (corrected: $P_{LBBBvsBaseline} < 0.001$, $P_{CRTvsBaseline} = NS$; non-corrected: $P_{LBBBvsBaseline} = NS$, $P_{CRTvsBaseline} = 0.028$). Our LBBB/CRT experimental model allowed controlling specific factors responsible for changes in mechanical dyssynchrony and therapy. We illustrated the importance of our quantification method to study these changes and their variability. Our findings confirm the importance of myocardial viability and of specific LBBB-related mechanical dyssynchrony patterns.

José Brugada and Bart Bijnens share senior authorship.

N. Duchateau (✉) · M. Sitges · A. Doltra · J. Fernández-Armenta · N. Solanes · M. Rigol · L. Gabrielli · E. Silva · A. Berruezo · L. Mont · J. Brugada
Arrhythmia, Resynchronization and Cardiac Imaging Unit, Hospital Clínic, Universitat de Barcelona, Calle Villarroel 170, 08036 Barcelona, Spain
e-mail: n.duchateaucistib@gmail.com;
nicolas.duchateau@upf.edu

N. Duchateau · M. Sitges · A. Doltra · J. Fernández-Armenta · N. Solanes · M. Rigol · L. Gabrielli · E. Silva · A. Berruezo · L. Mont · J. Brugada
Institut d'investigacions Biomèdiques August Pi i Sunyer, c/Rosselló 149-153, 08036 Barcelona, Spain

N. Duchateau · B. Bijnens
Universitat Pompeu Fabra,
c/Roc Boronat 138, 08018 Barcelona, Spain

L. Gabrielli
División de Enfermedades Cardiovasculares, Pontificia Universidad Católica de Chile, Marcoleta 367, 22354 3000 Santiago, Chile

A. Barceló
Sorin Group, Av/de les Corts Catalanes 8, Sant Cugat del Vallès, 08173 Barcelona, Spain

B. Bijnens
ICREA, Pg/Lluís Companys 23, 08010 Barcelona, Spain

Keywords Speckle-tracking · Myocardial strain · Myocardial velocity · Cardiac resynchronization therapy · Dyssynchrony

Introduction

Accurate characterization of myocardial motion and deformation patterns is essential for understanding changes in cardiac mechanics under the effect of disease and therapy [1]. Studies on Cardiac Resynchronization Therapy (CRT) mainly focused on the quantification of single value dyssynchrony indexes (e.g. time-to-event or peak measurements), and the qualitative description of the main pattern characteristics. In the first case, measurements are limited by the complexity of the mechanisms of cardiac dyssynchrony [2, 3], and the difficulty of defining CRT outcome and response as a dichotomic variable [4, 5]. In the second case, observations are qualitative and the pattern variability within groups of subjects is not directly measured [6–10].

In this study, we target the characterization of motion/deformation changes induced by pure left-bundle-branch-block (LBBB), and their evolution with CRT. Experimental models are relevant for such a purpose, as they allow controlling the factors responsible for such changes [11, 12]. To our knowledge, only one of these models included chronic infarct [13], but tested it for lead positioning purposes. In contrast, our study partially aims at studying its influence on patterns of mechanical (dys)synchrony.

Our priority is to improve the characterization of these changes. This consists in quantifying the whole morphology and variability of motion/deformation curves (i.e., the patterns) within the studied animals. Naturally, data differs between animals in terms of the timing of physiological events, number of frames, and anatomy. For this reason, we rely on recent methods for the statistical comparison of individuals, which can be easily transposed to our data [14]. These methods derive from the fields of computational anatomy and statistical atlases, and mainly consist in aligning all the studied data to a common system of spatiotemporal coordinates.

The contribution of our study is twofold: (i) we apply an appropriate comparison of motion and deformation patterns that overcomes the limits of previous studies on mechanical dyssynchrony; (ii) secondly, through an animal model of dyssynchrony with/without chronic infarct, we investigate the link between changes in mechanical dyssynchrony and induced electrical dyssynchrony (acute pure LBBB and following CRT). Two factors are tested and controlled by the experimental model: the relevance of correcting pure-LBBB dyssynchrony (non-infarcted animals), and the influence of an infarcted septum.

Methods

Animal model

Our study included 24 Landrace × Large White pigs [weight 37 (33–45) kg]. Two subpopulations were created: 12 animals without structural disease, and 12 with localized chronic infarct. The infarct was induced one-month before the LBBB induction, as a result of 90 min full occlusion of the left-anterior-descending coronary artery (LADi) [15]. Its position and extent were controlled 4 days before the LBBB induction using delayed-enhancement magnetic resonance (Magnetom-Symphony 1.5T, Siemens, Erlangen, Germany).

Acute LBBB was induced in all animals using radio-frequency ablation, guided through an electroanatomical mapping device (CARTO-XP, Biosense Webster, Diamond Bar, CA), so that QRS width increased $\geq 50\%$ with respect to baseline. This resulted in 4(3–7) burnings, at 25 mW during 30 s. This procedure is reproducible in inducing LBBB, as previously validated in [16] against other pacing protocols.

Two leads were implanted at baseline: right ventricle (RV, Bflex-RF45, Sorin Group, Milan, Italy) and left ventricle (LV, Situs-OTW, Sorin Group). The RV lead was located at the apex. The LV lead was implanted either by subxiphoid epicardial or via coronary sinus access, depending on the animal anatomy. The leads positioning was monitored by fluoroscopic guidance using a C-arm X-ray system (Arcadis Avantic, Siemens, Erlangen, Germany). Their position with respect to the infarct location was controlled a posteriori using the electroanatomical mapping data (earliest activation locations vs. bipolar voltage maps between 0.5 and 1.5 mV). Pacing was performed with a pacing system analyzer (ERA-3000, Biotronik, Berlin, Germany), and optimized after the ablation.

Further details about the leads positioning and the animal preparation protocol are given in [16]. Animal handling was approved by our Institutional Review Board and Ethics Committee, and conformed to current guidelines [17].

Echocardiography

An echocardiographic examination (Vivid-Q, GE Healthcare, Milwaukee, WI) was performed pre/post-ablation and during CRT using a transesophageal probe (6Tc-RS, GE Healthcare, 5 MHz) via subxiphoid epicardial access. Short-axis 2D views of the LV were acquired at papillary muscles level, during breath-hold (controlled through a respiratory device). Repeatability of the imaging plane between pre-ablation, post-ablation and CRT acquisitions was checked offline using a multi-view representation.

Machine settings (gain, time gain compensation, and compression) were adjusted for optimal visualization, including harmonic imaging. Sequences with insufficient image quality were discarded. Median frame rate and pixel size were of 67 [59–71] fps [heart rate: 80 (65–93) bpm] and $0.15 \times 0.15 \text{ mm}^2$, respectively.

Extraction of myocardial motion and deformation

Speckle-tracking protocol

Myocardial motion (displacement and velocities) and deformation (strain) were estimated by 2D speckle-tracking (Echopac-v110.1.2, GE Healthcare). The temporal region of interest was manually set to one cardiac cycle with approximately 100 ms additional margin around it. The myocardial border was manually segmented at end-systole, as required by the software interface (delineation of the endocardium and choice of a wall thickness).

Data export and post-processing

Data was exported with the “store full trace” option, without any spatiotemporal smoothing. Motion (radial/circumferential displacement and velocity) and deformation (circumferential strain) were computed along the myocardial centerline. Drift removal was used to achieve cyclic motion. The position of the myocardial centerline was corrected with respect to its center-of-mass to compensate probe motion.¹ No additional spatial/temporal smoothing was added.

Intra- and inter-observer variability

The repeatability of the speckle-tracking procedure was evaluated on 1 non-infarcted animal pre/post-ablation, and 1 LADi animal pre-ablation. Intra-observer variability was estimated by repeating the measurements 10 times. Inter-observer variability was obtained from 3 different observers. Finally, the inter-sequence variability was evaluated by repeating the measurements on another sequence.

Spatiotemporal alignment and data visualization

Data alignment

Speckle-tracking data is not immediately comparable between subjects. Indeed, physiological events happen at different instants, and sequences also differ in number of frames and anatomy. We used the method proposed in

Duchateau et al. [14, 18] to solve this (Fig. 1). This mainly consists in aligning all the studied data to a common system of spatiotemporal coordinates. *Temporal alignment* was based on the matching of physiological events.² *Spatial alignment* consisted in transporting the motion/deformation data of each subject to a reference anatomy (the anatomy of a given animal). The importance of this spatiotemporal alignment was already discussed [19, 20] and is illustrated in Fig. 2a, b. Technical details about the whole procedure and its validation can be found in Duchateau et al. [14, 18]. The implementation of the method was realized using Matlab-v.R2007a (MathWorks, Natick, MA), and is publically available.³

Data visualization

Motion and deformation patterns are visualized by means of color-coded maps, in which the horizontal axis stands for time (one cardiac cycle), and the vertical axis stands for the position along the myocardium (Fig. 1c). This visualization is similar to common commercial 2D speckle-tracking software. However, such software only offers descriptive visualization of an individual and does not allow quantitative comparison between subjects, contrary to our implementation.

Pattern analysis of motion/deformation curves

Single indexes

Differences in time-to-peak systolic strain between mid anteroseptal/inferolateral segments [21] were used as “conventional” indexes of mechanical dyssynchrony. Two types of more advanced indexes were also adapted from the ones recently proposed in Kydd et al. [22]: (i) the standard deviation of the time-to-peak circumferential strain, over the myocardial centerline ($\text{STD}_{\text{time-to-peak}}$), and (ii) the “wasted energy”, which corresponds to the average difference between peak circumferential strain and AVC circumferential strain, over the myocardial centerline. The relevance of such measurements is commented on in the “Discussion” section.

¹ Strain is a spatially differential measure and is not affected by this correction.

² The temporal alignment required the identification of 6 events per cycle. The onset of QRS (beginning and ending of the cycle) was identified on the ECG. Valve events (aortic/mitral valve opening/closure [AVO/AVC/MVO/MVC]) were identified using continuous-wave Doppler imaging on the corresponding valve, when possible, or visually on short-axis 2D views.

³ <http://nicolasduchateau.wordpress.com/downloads/>.

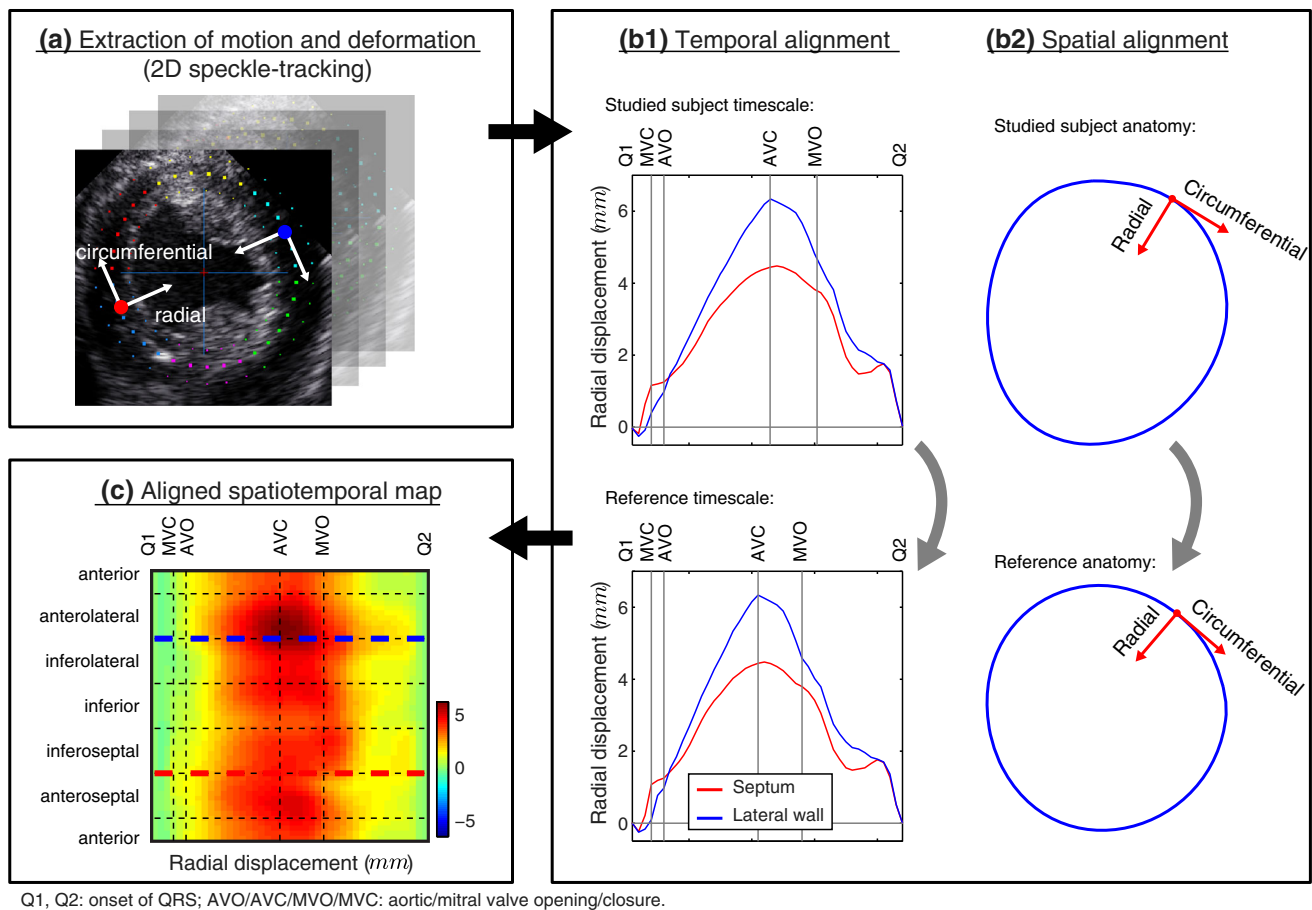


Fig. 1 Pipeline for the comparison of motion and deformation patterns

Local changes in mechanical patterns

Median and first/third quartiles radial displacement, radial velocity and circumferential strain were computed at each spatiotemporal location of the color-coded maps. They were used to quantify motion/deformation changes in the non-infarcted and LADi groups.

Global changes in cardiac function

Global circumferential strain corresponded to the average of the circumferential strain maps along their vertical dimension. We used the early-diastole shortening peak of global circumferential strain (negative isovolumic relaxation peak) to estimate changes in cardiac function.

Statistical analysis

Quantitative variables were expressed as median and first/third quartiles range. Non-parametric statistical tests were used for inter-groups comparison (Mann–Whitney *U* test) and paired data comparison (Wilcoxon signed-rank test).

p values <0.05 were considered statistically significant. All data were analyzed using SPSS-v.15.0 (SPSS Inc., Chicago, IL).

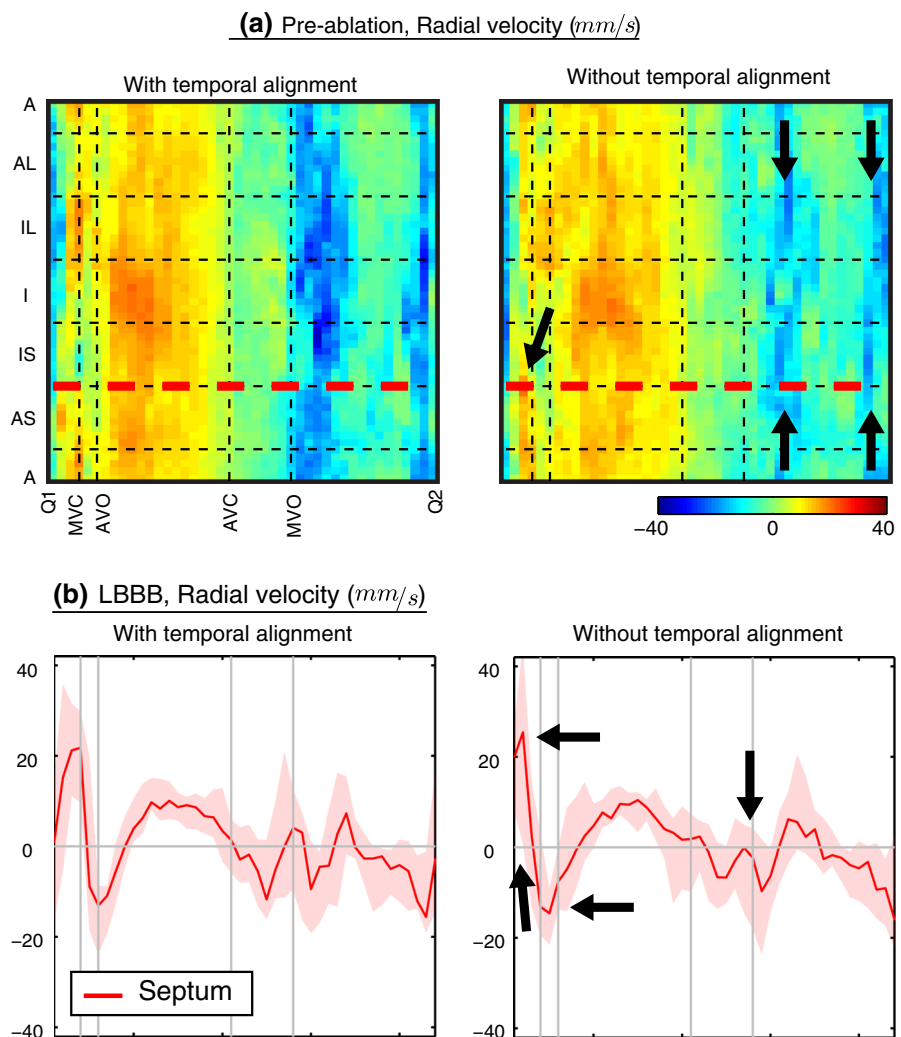
Results

Animal model

The characteristics of the studied animals are detailed in Table 1. In 22/24 animals, the successful induction of LBBB was confirmed by significant changes in the QRS morphology, axis and width [53 (46–56) ms vs. 80 (76–86) ms, *p* < 0.001]. This is illustrated in Fig. 3a on a non-infarcted animal. The 2/24 remaining animals developed a complete atrio-ventricular block (1 non-infarcted and 1 LADi) and were discarded.

LAD infarcts (N = 11) were located at the antero-septal level. More frequently affected segments were: mid-antero-septal (8/11), apical-anterior (8/11), and apical-septal (10/11). Other affected segments were: mid-anterior (2/11),

Fig. 2 Effect of temporal alignment. Prevention of artifacts (*black arrows*) in pre/post-ablation radial velocity (median, non-infarcted animals)



Q1, Q2: onset of QRS; AVO/AVC/MVO/MVC: aortic/mitral valve opening/closure.
 A: anterior; AL: anterolateral; IL: inferolateral; I: inferior; IS: inferoseptal; AS: anteroseptal.
 LBBB: left-bundle-branch-block.

mid-inferoseptal (3/11), apical-inferior (2/11), apical-lateral (1/11), and apex (3/11).

Intra- and inter-observer variability

The quantitative results for the repeatability experiments are summarized in Table 2 (standard deviation of the motion/deformation curves over the whole cycle and the whole myocardium) and Fig. 4 (repeated curves along the whole cycle at septal/lateral levels). Both indicate the low variability in the speckle-tracking measurements.

Pattern changes: conventional assessment

Fig. 3b highlights the presence after the ablation of a specific abnormal motion pattern of the septum, referred to

as septal flash (SF) [6]. It consists of early-systole fast inward/outward motion, as indicated by the yellow arrows. After the ablation, this pattern was observed in all the 11 non-infarcted animals, while it was harder to assess or absent in the 11 LADi ones. With CRT, mechanical dyssynchrony was partially or totally corrected in 10 of the 11 non-infarcted animals. Similarly, improvements in synchronicity were noted for 6 of the 11 LADi animals.

Table 1 includes measurements of mechanical dyssynchrony using time-to-peak systolic radial/circumferential strain. Large intra-population variability and no significant changes were observed with respect to pre-ablation data. This comes from the suboptimality of time-to-event indexes to characterize complex abnormal patterns [2, 3, 23], as also illustrated in Fig. 5. The wasted energy index led to similar observations. On the non-infarcted animals,

Table 1 Animal characteristics and single motion/deformation measurements

	Non-infarcted (N = 11)			LAD infarcted (N = 11)		
	Pre-ablation	LBBB	CRT	Pre-ablation	LBBB	CRT
Weight (kg)		35 [30/36]			45 [38/55]	
QRS width (ms)	55 [50/57]	84 [78/88] (<i>p</i> = 0.005)*	–	52 [45/55]	78 [75/86] (<i>p</i> = 0.005)*	–
Radial strain delay (ms)	0 [0/0]	0 [–15/29] (<i>p</i> = NS)*	0 [–38/14] (<i>p</i> = NS) ⁺	0 [–25/0]	0 [–99/17] (<i>p</i> = NS)*	0 [–105/16] (<i>p</i> = NS) ⁺
Circumferential strain delay (ms)	22 [–42/51]	47 [–103/101] (<i>p</i> = NS)*	49 [–38/91] (<i>p</i> = NS) ⁺	–28 [–51/0]	–71 [–177/98] (<i>p</i> = NS)*	–43 [–102/63] (<i>p</i> = NS) ⁺
STD _{time-to-peak} (% of cycle)	15 [14/19]	22 [20/26] (<i>p</i> = 0.006)*	20 [10/22] (<i>p</i> = NS) ⁺	17 [14/23]	19 [13/23] (<i>p</i> = NS)*	20 [14/25] (<i>p</i> = NS) ⁺
Wasted energy (%)	6.3 [5.3/7.6]	7.6 [7.1/8.3] (<i>p</i> = NS)*	5.9 [3.4/9.2] (<i>p</i> = NS) ⁺	5.6 [3.4/11.3]	6.1 [4.3/10.0] (<i>p</i> = NS)*	8.9 [5.0/12.0] (<i>p</i> = NS) ⁺
Global strain (%)	11.3 [9.6/14.6]	6.7 [6.0/8.1] (<i>p</i> = 0.003)*	8.9 [6.9/12.8] (<i>p</i> = NS) ⁺	8.2 [6.4/15.6]	5.9 [4.7/11.7] (<i>p</i> = 0.01)*	5.9 [3.9/11.0] (<i>p</i> = 0.01) ⁺

LAD left-anterior-descending, LBBB left-bundle-branch-block, CRT cardiac resynchronization therapy, NS Non-significant statistical difference (*p* value >0.05)

* Wilcoxon signed-rank test (LBBB vs. Pre-ablation)

⁺ Wilcoxon signed-rank test (CRT vs. Pre-ablation)

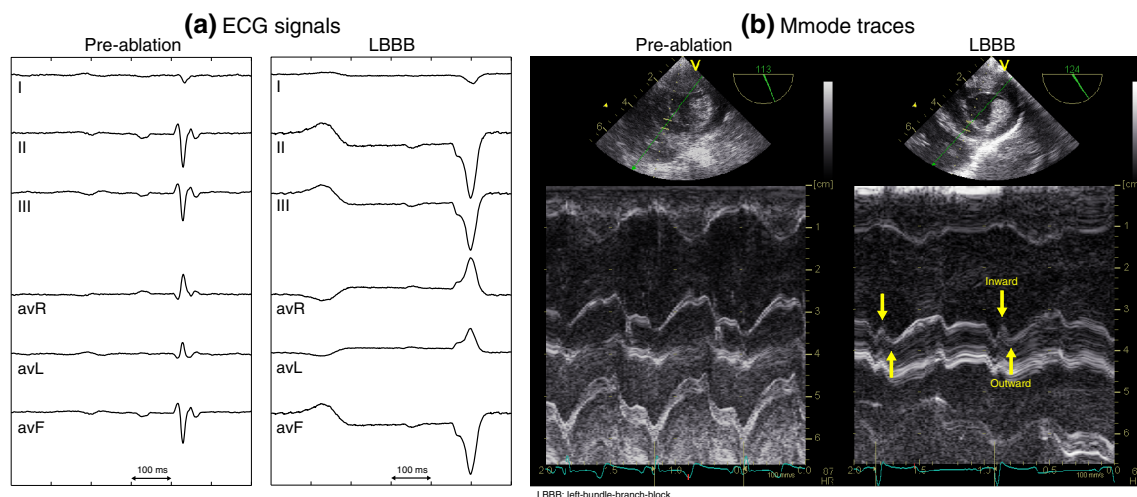


Fig. 3 Post-ablation changes on one non-infarcted animal. **a** ECG signals. **b** M-mode traces highlighting the presence of SF (yellow arrows)

significant differences were observed for the STD_{time-to-peak} index between pre- and post-ablation data, while differences between pre-ablation and CRT data were not significant. No significant differences were found for LADi animals. However, we doubt of the relevance of such a result, which is also based on time-to-event measurements.

Pattern changes: group-wise spatiotemporal analysis

Figure 6 represents the motion and deformation data for each subgroup of animals, pre/post-ablation and with CRT.

This consists of median and first/third quartiles curves at septal and lateral locations, and median spatiotemporal maps.

Non-infarcted animals (Fig. 6a)

After the ablation, the SF is visible on the displacement and velocity data (early-systole black arrows, septal level). It is accompanied by early-systole abnormal circumferential strain (peak shortening of the septum and lateral wall stretching during the isovolumic contraction). Reduction of

Table 2 Variability of the speckle-tracking procedure

		Non-infarcted		
		LAD infarct		Pre-ablation
		Pre-ablation	LBBB	
Radial displacement (mm)	Intra-obs.	0.2 ± 0.1	0.2 ± 0.1	0.1 ± 0.1
	Inter-seq.	0.5 ± 0.4	0.3 ± 0.3	0.4 ± 0.4
	Inter-obs.	0.4 ± 0.2	0.4 ± 0.3	1.0 ± 0.7
Radial velocity (mm/s)	Intra-obs.	1.9 ± 1.5	3.3 ± 2.7	1.5 ± 1.5
	Inter-seq.	7.0 ± 6.5	7.1 ± 7.3	4.5 ± 4.2
	Inter-obs.	4.6 ± 4.1	4.4 ± 3.6	8.0 ± 6.3
Circumferential strain (%)	Intra-obs.	2.2 ± 1.1	2.2 ± 1.3	0.8 ± 0.6
	Inter-seq.	3.7 ± 3.7	2.9 ± 2.2	0.3 ± 0.2
	Inter-obs.	3.8 ± 2.9	3.3 ± 2.3	5.0 ± 3.9

Intra-observer, inter-observer, and inter-sequence variability (standard deviation of the motion/deformation curves over the whole cycle and the myocardial centerline)

LAD left-anterior-descending, LBBB left-bundle-branch-block

systolic and diastolic velocities, loss of synchronicity (absence of vertical symmetry/uniformity of the maps), and post-systolic abnormal motion (early-diastole black arrows) are also observed. With CRT, SF has disappeared, synchronicity has been restored (improved vertical symmetry/uniformity of the maps), and the contraction/relaxation patterns resemble to the pre-ablation ones.

LADi animals (Fig. 6b)

High variability of the circumferential strain curves is observed. This reflects the heterogeneity of infarct extent in this subgroup: fully or partially infarcted septum at the papillary muscles level versus a more apical/anterior infarct. Motion is also slightly altered at the infarct location before the ablation. Velocities are lower before the ablation, in comparison with the non-infarcted animals. After the ablation, few changes are observed. No SF pattern is visible. Synchronicity is partially preserved (vertical symmetry of the maps), but motion is reduced. Post-systolic abnormal motion (early-diastole black arrows) is also observed. Few changes happen with CRT. Strain is partially improved in the lateral wall, which coincides with the non-infarcted zone.

Changes in cardiac function

Global circumferential strain values are summarized in Table 1. Non-infarcted animals showed lower global deformation after the ablation, which was almost restored with CRT. The LADi subpopulation showed a larger dispersion of global strain values before the ablation, which confirms the observations of Fig. 6b. Global strain values were lower before the ablation, worsened with LBBB and were not restored with CRT.

These results are confirmed when animals are grouped according to CRT-induced improvements. Partial or total correction of LBBB-induced abnormal patterns (10 non-infarcted and 6 LADi animals) was accompanied by the restoration of cardiac function [11.0 (8.2–15.4) % (pre-ablation) vs. 7.1 (5.3–8.3) %, $p < 0.001$ (LBBB) and 9.5 (6.3–12.5) %, $p = \text{NS}^4$ (CRT)]. On the contrary, non-correction of dyssynchrony and undetermined changes (1 non-infarcted and 5 LADi animals) correlated with a lack of improvement of cardiac function [9.2 (6.8–14.5) % (pre-ablation) vs. 5.9 (4.9–9.1) %, $p = \text{NS}$ (LBBB) and 5.0 (3.7–6.3) %, $p = 0.028$ (CRT)].

Discussion

In this study, we used local motion and deformation data to quantify mechanical (dys)synchrony patterns induced by LBBB and following CRT in an animal model of dyssynchrony with/without chronic infarct. Our objectives were (i) to apply an appropriate method to compare motion and deformation patterns at each stage of the experiments; and (ii) to study the link between changes in mechanical dyssynchrony and induced electrical dyssynchrony (acute pure LBBB and following CRT).

Conventional assessment of mechanical dyssynchrony

The limits of conventional methods for the assessment of mechanical dyssynchrony have been widely debated [24, 25]. The abundance of publications and extensively advertised multi-centric studies made the usefulness of myocardial mechanics controversial [2, 3]. Single indexes

⁴ NS: Non-significant statistical difference (p value > 0.05).

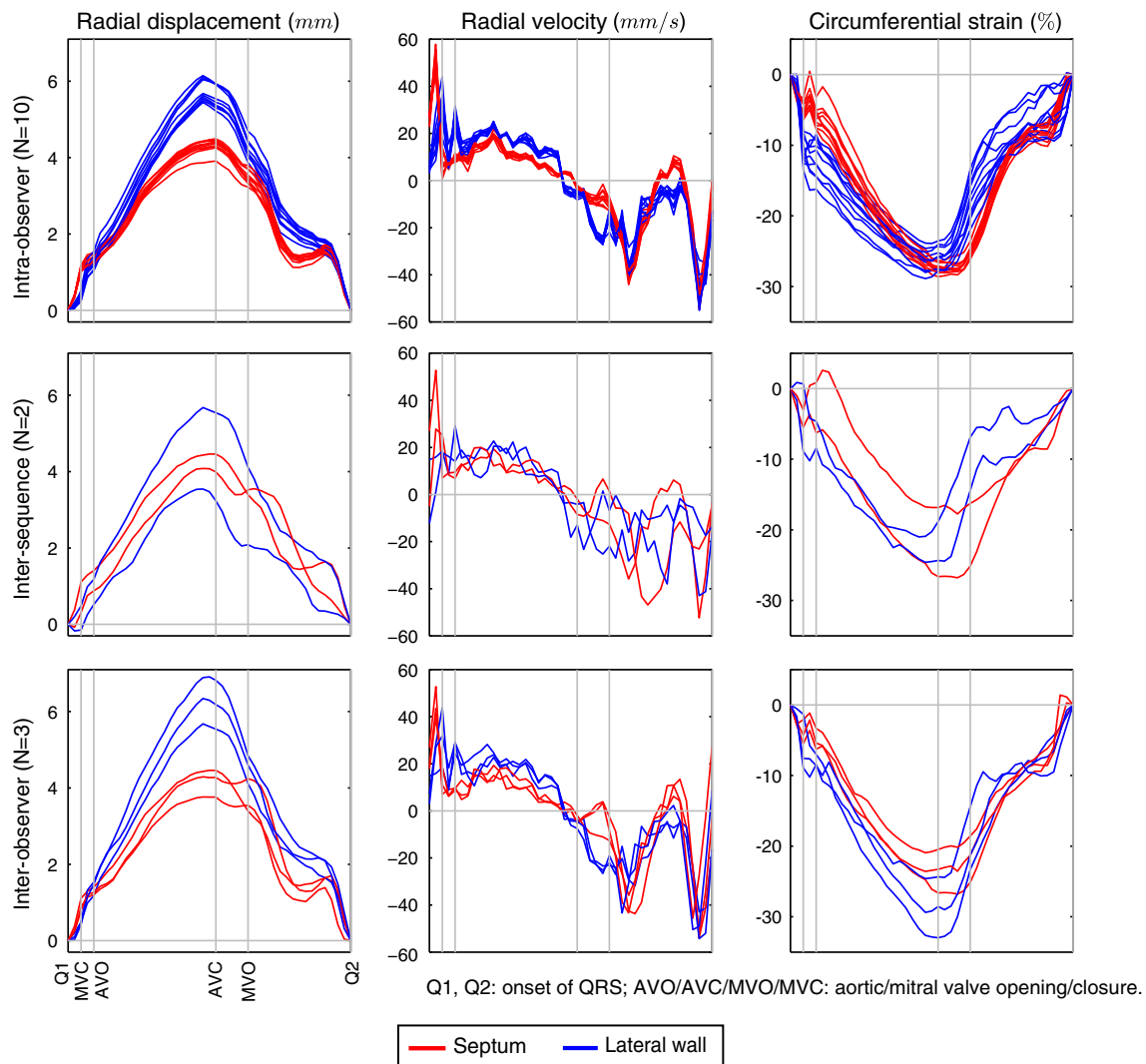


Fig. 4 Repeatability of the computations illustrated for one non-infarcted animal

such as time-to-event or single location values discard the complexity of the patterns observed (Fig. 5) [23]. A similar remark can be made for more elaborated methods, such as curve analysis (e.g. cross-correlation [26] or Fourier analysis [27]) and more advanced indexes (e.g. radial discoordination [22, 28] or the wasted energy [22]). Note that these limitations come from the analysis that is made and not from the images. They are independent of the imaging technique, and therefore not specific to speckle-tracking echocardiography.

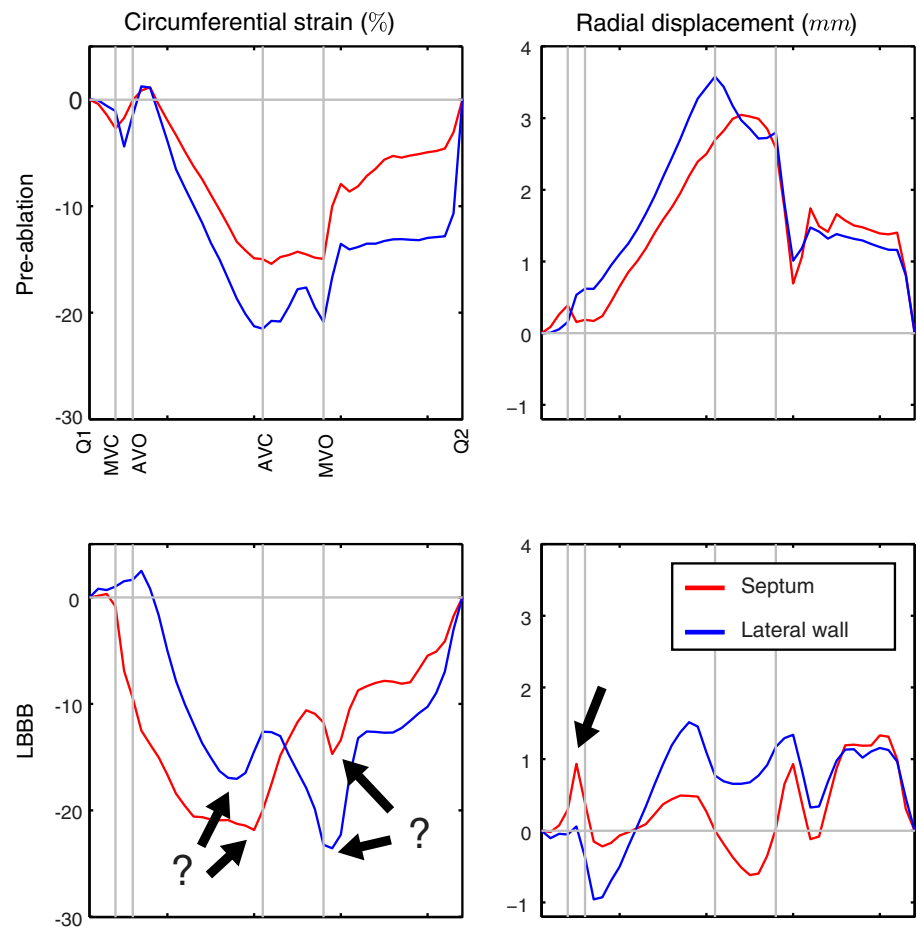
Pattern analysis

Pattern-based observations were recently reported in the context of CRT to address the problem in a more comprehensive way [6–10]. However, most works are still limited to qualitative pattern description, or single pattern-

specific measurements (e.g. peak magnitude of SF, systolic rebound shortening and pre-stretch [7, 8], or apical transverse motion for rocking [9]). In contrast, our method performs a more complete quantitative analysis, and includes data of multiple types (displacement, velocities and strain). Moreover, this data is studied locally all along the myocardial centerline and not only in predefined regions such as myocardial segments. The usefulness of the method has been demonstrated to characterize the variety of motion patterns that can be observed along the myocardium [20, 29].

Our approach has a second advantage for this type of studies. It allows the computation of the pattern morphology and variability within a given population. Looking at the average pattern confirms qualitative observations previously made [6–10]. Looking at its variability is essential to understand the reproducibility of the clinical

Fig. 5 Difficulty of characterizing dyssynchrony by single measurements (peak identification), on one non-infarcted animal



Q1, Q2: onset of QRS; AVO/AVC/MVO/MVC: aortic/mitral valve opening/closure. LBBB: left-bundle-branch-block.

observations. Both points are important for the clinical observer performing population studies. However, such a pattern analysis is only possible if data are compared at the same locations along the myocardium and the same temporal instants. With our method, data have been spatio-temporally aligned to a same reference system of coordinates. Such computations are not possible with any other existing method, and in particular with the current commercial speckle-tracking software. This relatively new pattern quantification was initially proposed in Duchateau et al. [14] and applied to the comparison of velocity patterns to those of a normal population [14, 18–20, 29]. In the present study, we extended this framework to other parameters than velocities (displacement and strain), and illustrated it in our experimental model.

Animal model

Our method was applied to an experimental closed-chest model of pure LBBB undergoing CRT [16]. Such a model

(in comparison with clinical studies) allows controlling some of the factors responsible for changes in mechanical dyssynchrony and following outcome. In particular, the non-infarcted animals before the ablation and the infarcted ones before the infarct procedure have normal cardiac function, with no antecedent of cardiac disease. This differs from patients that may show age-related physical and functional alterations. Thus, in non-infarcted animals, only the relevance of correcting LBBB-induced dyssynchrony was tested, while a second factor (infarcted septum) was tested on the LADi animals.

Previous animal studies reported the changes in dyssynchrony induced by LBBB and following CRT [11, 12]. The closest models from our study were based on dogs. We preferred to perform on pigs for cost-effectiveness and experimental facilities reasons. Our observations on LBBB-related changes confirm the ones described in the literature. Our contribution is on quantitative curve analysis, and in particular on the characterization of the pattern morphology and its variability within a given population.

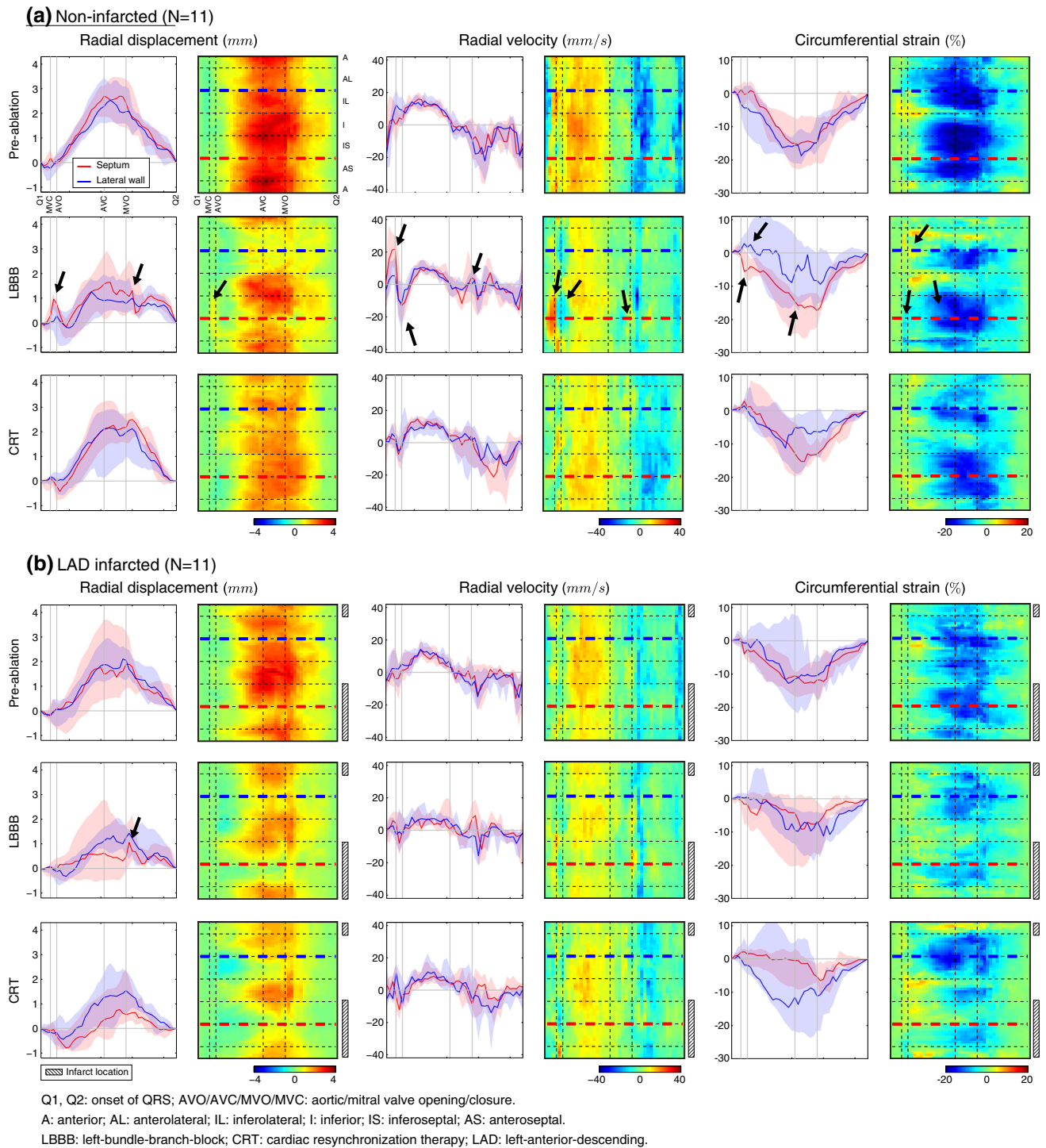


Fig. 6 Radial displacement, velocity and circumferential strain for each subgroup. Septal/lateral curves (median and first/third quartiles) and full spatiotemporal (median) maps. *Black arrows* highlight the

presence of SF, double-peaked systolic septal shortening, early-systole lateral wall stretch and post-systolic abnormal motion

Furthermore, to our knowledge, only one of the models mentioned in the literature included chronic infarct [13] but for lead positioning purposes, while our study examines its influence on patterns of mechanical dyssynchrony.

Changes in mechanical dyssynchrony patterns

The findings of our study confirm that a very specific pattern of mechanical dyssynchrony derives from pure

LBBB. This pattern is visible on both motion and deformation data (Figs. 3, 6). It consists of a fast inward/outward motion of the septum during the isovolumic contraction, and early-systolic peak shortening of the septum. Stretching of the lateral wall is observed during the same temporal period. We also noticed the presence of LBBB-induced post-systolic abnormal motion, as discussed elsewhere [30]. Similar patterns were previously described [31–34], and recently referred to as septal flash [6], septal rebound stretch [7, 8], or apical rocking [9]. Our experimental results confirm hypotheses about their link with electrical conduction delays and LBBB. This was recently discussed using computer simulations [7, 35], experimental [11–13, 36] and clinical data [7, 37, 38]. Further work is expected to fully understand how these specific electrical and mechanical alterations interact.

The LBBB-induced dyssynchrony patterns are observed in all the non-infarcted animals (Fig. 6). However, patterns are less marked than in patients' sequences. In particular, the late systolic dyssynchrony and lateral wall stretch are sometimes subtle to assess. This may come from the electrical dyssynchrony induced on the animals. QRS width increased by more than 50 %, but its post-ablation duration is of 83 ± 10 ms, which is within the range of normal durations for human data. The use of dobutamine tests may probably increase the patterns magnitude [39], but it is not clear if the QRS duration should change. The analysis of electroanatomical data may complement this by looking for the presence of conduction block, as observed in humans [37]. One possible difference with human data may be in how ablation actually damages the left-bundle-branch (punctual burnings in pigs, against more diffuse natural damage in patients). The lack of delay between the induction of LBBB and imaging may be another reason for this. No time is left for remodeling processes, while remodeling may influence the mechanical dyssynchrony patterns of patients.

Changes in cardiac function

We reported that in the absence of structural disease, the correction of SF resulted in a significant improvement of cardiac function in all pigs, while the opposite was also true (the lack of SF correction in one non-infarcted animal resulted in no improvement of cardiac function). These results support previous observations on the relation between improvements of cardiac function, reverse remodeling and volume response to CRT [6, 37].

Local viability of the myocardium

We also demonstrated that a localized infarct can strongly limit the presence of SF after the ablation. In case of LADi,

the viability and contractility of the septum are strongly decreased at the scar location. The motion and deformation patterns of the septum are therefore altered, as previously described [6, 7, 20]. When CRT is applied, the presence of a LADi may be a possible cause of non-response, as electrical dyssynchrony is not anymore the only factor of changes in cardiac contraction.

Implications

From an *image analysis/quantification point-of-view*, our approach provides a complete characterization of motion and deformation patterns that is difficult to obtain with more conventional measurements. Our observations include spatiotemporal data alignment and efficient visualization tools for studying the patterns morphology and variability within a given population. This may be challenging in clinical practice, in particular with the limited access to such post-processing tools. Our approach recommends at least including qualitative pattern observations in the analysis, as performed in [6–10]. Quantitative analysis should consider comparing data at the same locations along the myocardium and the same physiological instants. The former may be achieved by segmental analysis, as provided in a majority of commercial speckle-tracking software. The latter is more challenging. Temporal measurements should at least be normalized by the length of the cardiac cycle, and if possible the length of the systolic/diastolic phases. We also remind that our post-processing tools are publically available (see Footnote 3).

From a *clinical point-of-view*, our findings confirm the importance of the viability of the myocardium and of specific mechanical dyssynchrony patterns related to LBBB. In case of pure-LBBB and the lack of other external factors, CRT is likely to be effective, if normal motion and deformation are restored. Infarcted patients may benefit from CRT, but with a higher uncertainty due to the complexity of the infarct implications. For clinical practice, this means being critical with respect to the classical inclusion criteria for CRT, and conventional methods for assessing mechanical dyssynchrony. Pattern observations allow better understanding of the complex LBBB/CRT-induced changes, as also considered qualitatively in [6–10].

Additional comments and limitations

Our study used 2D views at the papillary muscles level. Additional 2D/3D views could improve our understanding of the patterns observed [40]. However, these views were not available in our experimental protocol with sufficient image quality and spatiotemporal resolution.

The variability of the experimental protocol is a limitation. This includes the quality of the ablation procedure

(actual damage made to the left-bundle-branch), the infarct extent, and the leads location.

Finally, it should be reminded that this study uses an experimental model built for understanding purposes. No other forms of heart failure than dyssynchrony and infarction were considered (e.g. no rapid pacing was applied). Similarly, no additional factors that may influence CRT response were studied (e.g. heart failure, the lack of contractile reserve, the presence of atrial fibrillation, or a poor clinical condition at baseline). These aspects should be taken into account when looking at clinical data [20, 29].

Conclusion

The use of a LBBB/CRT experimental model allowed controlling specific factors responsible for changes in mechanical dyssynchrony and therapy. We illustrated the importance of our quantification method, based on curve analysis rather than single measurements, to study these changes and their variability. Our study complements previous qualitative observations on specific LBBB/CRT-induced changes, aiming at a better understanding of motion and deformation in CRT candidates.

Acknowledgments This work was partially supported by the Centre for the Development of Industrial Technology, Madrid, Spain (cvREMEDIATION CEN-20091044) and the European Union Seventh Framework Programme (VP2HF FP7-2013-611823). AD had a post-residency grant from Fundació Clínic, Barcelona, Spain. The authors acknowledge David Andreu and Santiago Sotes (Hospital Clínic, Barcelona, Spain), Daniel Traver (Biosense Webster, Barcelona, Spain), Laia Bayarri and Filippo Ziglio (Sorin Group, Barcelona/Milan, Spain/Italy) for their support on the experimental devices.

Conflict of interest None declared.

References

- Bijnens BH, Cikes M, Butakoff C, Sitges M, Crispi F (2012) Myocardial motion and deformation: what does it tell us and how does it relate to function? *Fetal Diagn Ther* 32:5–16. doi:10.1159/000335649
- Fornwalt BK, Delfino JG, Sprague WW, Oshinski JN (2009) It's time for a paradigm shift in the quantitative evaluation of left ventricular dyssynchrony. *J Am Soc Echocardiogr* 22:672–676. doi:10.1016/j.echo.2009.04.012
- Fornwalt BK (2011) The dyssynchrony in predicting response to cardiac resynchronization therapy: a call for change. *J Am Soc Echocardiogr* 24:180–184. doi:10.1016/j.echo.2010.12.015
- Fornwalt BK, Sprague WW, BeDell P, Suever JD, Gerritse B, Merlino JD, Fyfe DA, León AR, Oshinski JN (2010) Agreement is poor among current criteria used to define response to cardiac resynchronization therapy. *Circulation* 121:1985–1991. doi:10.1161/CIRCULATIONAHA.109.910778
- Cleland JG, Ghio S (2012) The determinants of clinical outcome and clinical response to CRT are not the same. *Heart Fail Rev* 17:755–766. doi:10.1007/s10741-011-9268-9
- Parsai C, Bijnens B, Sutherland GR, Baltabaeva A, Claus P, Marciniak M, Paul V, Scheffer M, Donal E, Derumeaux G, Anderson L (2009) Toward understanding dyssynchrony to cardiac resynchronization therapy: left ventricular dyssynchrony is only one of multiple mechanisms. *Eur Heart J* 30:940–949. doi:10.1093/eurheartj/ehn481
- Leenders GE, Lumens J, Cramer MJ, De Boeck BW, Doevendans PA, Delhaas T, Prinzen FW (2012) Septal deformation patterns delineate mechanical dyssynchrony and regional differences in contractility: analysis of patient data using a computer model. *Circ Heart Fail* 5:87–96. doi:10.1161/CIRCHEARTFAILURE.111.962704
- De Boeck BW, Teske AJ, Meine M, Leenders GE, Cramer MJ, Prinzen FW, Doevendans PA (2009) Septal rebound stretch reflects the functional substrate to cardiac resynchronization therapy and predicts volumetric and neurohormonal response. *Eur J Heart Fail* 11:863–871. doi:10.1093/eurjhf/hfp107
- Szulik M, Tillekaerts M, Vangeel V, Ganame J, Willems R, Lenarczyk R, Rademakers F, Kalarus Z, Kukulski T, Voigt JU (2010) Assessment of apical rocking: a new, integrative approach for selection of candidates for cardiac resynchronization therapy. *Eur J Echocardiogr* 11:863–869. doi:10.1093/ejehocardiography/jeq081
- Risum N, Jons C, Olsen NT, Fritz-Hansen T, Bruun NE, Hojgaard MV, Valeur N, Kronborg MB, Kisslo J, Sogaard P (2012) Simple regional strain pattern analysis to predict response to cardiac resynchronization therapy: rationale, initial results, and advantages. *Am Heart J* 163:697–704. doi:10.1016/j.ahj.2012.01.025
- Prinzen FW, Peschar M (2002) Relation between the pacing induced sequence of activation and left ventricular pump function in animals. *Pacing Clin Electrophysiol* 25:484–498. doi:10.1046/j.1460-9592.2002.00484.x
- Strik M, van Middendorp LB, Vernooij K (2012) Animal models of dyssynchrony. *J Cardiovasc Transl Res* 5:135–145. doi:10.1007/s12265-011-9336-5
- Rademakers LM, van Kerckhoven R, van Deursen CJ, Strik M, van Hunnik A, Kuiper M, Lampert A, Klersy C, Leyva F, Auricchio A, Maessen JG, Prinzen FW (2010) Myocardial infarction does not preclude electrical and hemodynamic benefits of cardiac resynchronization therapy in dyssynchronous canine hearts. *Circ Arrhythm Electrophysiol* 3:361–368. doi:10.1161/CIRCEP.109.931865
- Duchateau N, De Craene M, Piella G, Silva E, Doltra A, Sitges M, Bijnens BH, Frangi AF (2011) A spatiotemporal statistical atlas of motion for the quantification of abnormal myocardial tissue velocities. *Med Image Anal* 15:316–328. doi:10.1016/j.media.2010.12.006
- Rigol M, Solanes N, Farré J, Roura S, Roqué M, Berrueto A, Bellera N, Novensà L, Tamborero D, Prat-Vidal C, Huzman MA, Batlle M, Hoefsloot M, Sitges M, Ramírez J, Dantas AP, Merino A, Sanz G, Brugada J, Bayés-Genís A, Heras M (2010) Effects of adipose tissue-derived stem cell therapy after myocardial infarction: impact of the route of administration. *J Card Fail* 16:357–366. doi:10.1016/j.cardfail.2009
- Rigol M, Solanes N, Fernandez-Armenta J, Silva E, Doltra A, Duchateau N, Barcelo A, Gabrielli L, Bijnens B, Berrueto A, Brugada J, Sitges M (2013) Development of a swine model of left bundle branch block for experimental studies of cardiac resynchronization therapy. *J Cardiovasc Transl Res* 6:616–622. doi:10.1007/s12265-013-9464-1
- National Research Council (2011) Guide for the care and use of laboratory animals, 8th edn. The National Academies Press, Washington, DC
- Duchateau N, De Craene M, Pennec X, Merino B, Sitges M, Bijnens BH (2012) Which reorientation framework for the atlas-based comparison of motion from cardiac image sequences? In:

- Proceedings of spatio-temporal image analysis for longitudinal and time-series image data, MICCAI'12 workshop. Springer LNCS vol. 7570, pp 25–37. doi:[10.1007/978-3-642-33555-6_3](https://doi.org/10.1007/978-3-642-33555-6_3)
19. De Craene M, Duchateau N, Tobon-Gomez C, Ghafaryasl B, Piella G, Rhode KS, Frangi AF (2012) SPM to the heart: mapping of 4D continuous velocities for motion abnormality quantification. In: Proceedings of IEEE international symposium on bio-medical imaging, pp 454–457. doi:[10.1109/ISBI.2012.6235582](https://doi.org/10.1109/ISBI.2012.6235582)
 20. Duchateau N, Doltra A, Silva E, De Craene M, Piella G, Castel MA, Mont L, Brugada J, Frangi AF, Sitges M (2012) Atlas-based quantification of myocardial motion abnormalities: added-value for the understanding the effect of cardiac resynchronization therapy. *Ultrasound Med Biol* 38:2186–2197. doi:[10.1016/j.ultrasmedbio.2012.08.009](https://doi.org/10.1016/j.ultrasmedbio.2012.08.009)
 21. Delgado V, Ypenburg C, van Bommel RJ, Tops LF, Mollema SA, Marsan NA, Bleeker GB, Schalij MJ, Bax JJ (2008) Assessment of left ventricular dyssynchrony by speckle tracking strain imaging comparison between longitudinal, circumferential, and radial strain in cardiac resynchronization therapy. *J Am Coll Cardiol* 51:1944–1952. doi:[10.1016/j.jacc.2008.02.040](https://doi.org/10.1016/j.jacc.2008.02.040)
 22. Kydd AC, Khan FZ, O'Halloran D, Pugh PJ, Virdee MS, Dutka DP (2013) Radial strain delay based on segmental timing and strain amplitude predicts left ventricular reverse remodeling and survival after cardiac resynchronization therapy. *Circ Cardiovasc Imaging* 6:177–184. doi:[10.1161/CIRCIMAGING.112.000191](https://doi.org/10.1161/CIRCIMAGING.112.000191)
 23. Anderson LJ, Miyazaki C, Sutherland GR, Oh JK (2008) Patient selection and echocardiographic assessment of dyssynchrony in cardiac resynchronization therapy. *Circulation* 117:1023–2009. doi:[10.1161/CIRCULATIONAHA.107.721332](https://doi.org/10.1161/CIRCULATIONAHA.107.721332)
 24. Delgado V, Bax JJ (2011) Assessment of systolic dyssynchrony for cardiac resynchronization therapy is clinically useful. *Circulation* 123:640–655. doi:[10.1161/CIRCULATIONAHA.110.954404](https://doi.org/10.1161/CIRCULATIONAHA.110.954404)
 25. Sung RK, Foster E (2011) Assessment of systolic dyssynchrony for cardiac resynchronization therapy is not clinically useful. *Circulation* 123:656–662. doi:[10.1161/CIRCULATIONAHA.110.954420](https://doi.org/10.1161/CIRCULATIONAHA.110.954420)
 26. Silva E, Sitges M, Doltra A, Mont L, Vidal B, Castel MA, Tolosana JM, Berruetez A, González Juanatey JR, Brugada J (2010) Analysis of temporal delay in myocardial deformation throughout the cardiac cycle: utility for selecting candidates for cardiac resynchronization therapy. *Heart Rhythm* 7:1580–1586. doi:[10.1016/j.hrthm.2010.06.034](https://doi.org/10.1016/j.hrthm.2010.06.034)
 27. Bertola B, Rondano E, Sulis M, Sarasso G, Piccinino C, Marti G, Devecchi P, Magnani A, Francalacci G, Marino PN (2009) Cardiac dyssynchrony quantitated by time-to-peak or temporal uniformity of strain at longitudinal, circumferential, and radial level: implications for resynchronization therapy. *J Am Soc Echocardiogr* 22:665–671. doi:[10.1016/j.echo.2009.03.010](https://doi.org/10.1016/j.echo.2009.03.010)
 28. Chan YH, Kuo CT, Yeh YH, Wu LS, Wang CL, Ho WJ, Hsu LA (2013) Incremental value of radial discoordination index for the prediction of response to cardiac resynchronization therapy. *Eur Heart J* 14:213–222. doi:[10.1093/ehjci/jes112](https://doi.org/10.1093/ehjci/jes112)
 29. Tobon-Gomez C, Duchateau N, Sebastian R, Marchesseau S, Camara O, Donal E, De Craene M, Pashaei A, Relan J, Steghofer M, Lamata P, Delingette H, Duckett S, Garreau M, Hernandez A, Rhode KS, Sermesant M, Ayache N, Leclercq C, Razavi R, Smith NP, Frangi AF (2013) Understanding the mechanisms amenable to CRT response: from pre-operative multimodal image data to patient-specific computational models. *Med Biol Eng Comput* 51:1235–1250. doi:[10.1007/s11517-013-1044-7](https://doi.org/10.1007/s11517-013-1044-7)
 30. Ring M, Persson H, Mejhert M, Edner M (2007) Post-systolic motion in patients with heart failure—a marker of left ventricular dyssynchrony? *Eur J Echocardiogr* 8:352–359. doi:[10.1016/j.euje.2006.07.006](https://doi.org/10.1016/j.euje.2006.07.006)
 31. McDonald IG (1973) Echocardiographic demonstration of abnormal motion of the interventricular septum in left bundle branch block. *Circulation* 48:272–280. doi:[10.1161/01.CIR.48.2.272](https://doi.org/10.1161/01.CIR.48.2.272)
 32. Dillon JC, Chang S, Feigenbaum H (1974) Echocardiographic manifestations of left-bundle branch-block. *Circulation* 49:876–880. doi:[10.1161/01.CIR.49.5.876](https://doi.org/10.1161/01.CIR.49.5.876)
 33. Little WC, Reeves RC, Arciniegas J, Katholi RE, Rogers EW (1982) Mechanism of abnormal inter-ventricular septal motion during delayed left-ventricular activation. *Circulation* 65:1486–1491. doi:[10.1161/01.CIR.65.7.1486](https://doi.org/10.1161/01.CIR.65.7.1486)
 34. Grines CL, Bashore TM, Boudoulas H, Olson S, Shafer P, Wooley CF (1989) Functional abnormalities in isolated left bundle branch block. The effect of interventricular asynchrony. *Circulation* 79:845–853. doi:[10.1161/01.CIR.79.4.845](https://doi.org/10.1161/01.CIR.79.4.845)
 35. Kerckhoffs RC, Omens JH, McCulloch AD (2012) Mechanical discoordination increases continuously after the onset of left bundle branch block despite constant electrical dyssynchrony in a computational model of cardiac electromechanics and growth. *Europace* 14:v65–v72. doi:[10.1093/europace/eus274](https://doi.org/10.1093/europace/eus274)
 36. Gjesdal O, Remme EW, Opdahl A, Skulstad H, Russell K, Kongsgaard E, Edvardsen T, Smiseth OA (2011) Mechanisms of abnormal systolic motion of the interventricular septum during left bundle-branch block. *Circ Cardiovasc Imaging* 4:264–273. doi:[10.1161/CIRCIMAGING.110.961417](https://doi.org/10.1161/CIRCIMAGING.110.961417)
 37. Duckett SG, Camara O, Ginks MR, Bostock J, Chinchapatnam P, Sermesant M, Pashaei A, Lambiase PD, Gill JS, Carr-White GS, Frangi AF, Razavi R, Bijns BH, Rinaldi CA (2012) Relationship between endocardial activation sequences defined by high-density mapping to early septal contraction (septal flash) in patients with left bundle branch block undergoing cardiac resynchronization therapy. *Europace* 14:99–106. doi:[10.1093/europace/eur235](https://doi.org/10.1093/europace/eur235)
 38. Risum N, Strauss D, Sogaard P, Loring Z, Fritz-Hansen T, Bruun NE, Wagner G, Kisslo J (2013) Left bundle-branch block: the relationship between electrocardiogram electrical activation and echocardiography mechanical contraction. *Am Heart J* 166:340–348. doi:[10.1016/j.ahj.2013.04.005](https://doi.org/10.1016/j.ahj.2013.04.005)
 39. Parsai C, Baltabaeva A, Anderson L, Chaparro M, Bijns BH, Sutherland GR (2009) Low-dose dobutamine stress echo to quantify the degree of remodelling after cardiac resynchronization therapy. *Eur Heart J* 30:950–958. doi:[10.1093/eurheartj/ehp050](https://doi.org/10.1093/eurheartj/ehp050)
 40. Duchateau N, Bijns BH, D'hooge J, Sitges M (2013) Three-dimensional assessment of cardiac motion and deformation. In: Shiota T (ed) 3D echocardiography, 2nd edn. CRC Press, Boca Raton, pp 201–213